Pacific Northwest
NATIONAL LABORATORY

PNNL-34393

Extending Magnetic Core Shell Nanoparticle Extraction Technology to Cesium and Antimony Removal from Geothermal Brines in New Zealand

Final Project Report

June 2023

Minbum Kim
Satish K. Nune
Jierui Yu
Jian Liu
Praveen K. Thallapally

U.S. DEPARTMENT OF ENERGY

Prepared for the U.S. Department of Energy
under Contract DE-AC05-76RL01830

DISCLAIMER

PACIFIC NORTHWEST NATIONAL LABORATORY
operated by
BATTELLE
for the
UNITED STATES DEPARTMENT OF ENERGY
under Contract DE-AC05-76RL01830

Printed in the United States of America

Available to DOE and DOE contractors from the Office of Scientific and Technical Information,
P.O. Box 62, Oak Ridge, TN 37831-0062
www.osti.gov
ph: (865) 576-8401
fax: (865) 576-5728
email: reports@osti.gov

Available to the public from the National Technical Information Service
5301 Shawnee Rd., Alexandria, VA 22312
ph: (800) 553-NTIS (6847)
or (703) 605-6000
email: info@ntis.gov
Online ordering: http://www.ntis.gov

PNNL-34393

Extending Magnetic Core Shell Nanoparticle Extraction Technology to Cesium and Antimony Removal from Geothermal Brines in New Zealand

June 2023

Minbum Kim

Satish K. Nune

Jierui Yu

Jian Liu

Praveen K. Thallapally

Prepared for
the U.S. Department of Energy
under Contract DE-AC05-76RL01830

Pacific Northwest National Laboratory
Richland, Washington 99354

Summary

Our industrial client (Geo40) has developed and deployed a process to remove silica from geothermal fluids and produce a high-margin specialty colloidal silica product comparable to those of market leaders. Geo40 now wishes to explore opportunities to extend their mineral extraction operations to other elements that are present in these brines using magnetic core shell approach which is licensed to Moselle Technologies LLC. Geo40 has identified cesium (Cs) that is present in Ohaaki brines (pH ~8–8.5) at parts per million levels and could be sold to customers if it could be produced at an attractive price. With support from the Department of Energy's (DOE's) Geothermal Technologies Office, a simple and highly cost-effective magnetic nanofluid method for extraction of rare earth elements (REEs) from geothermal brine solutions has been developed and demonstrated at the laboratory bench scale at Pacific Northwest National Laboratory (PNNL). Core shell sorbent particles are produced using an iron oxide core particle, which is used to anchor and grow a surrounding adsorbent shell functionalized with a chelating ligand that selectively binds REEs. We extended PNNL's work by exploring new sorbent shells that are highly selective for Cs. Uptake of Cs was measured as a function of exposure time by analyzing solution samples extracted from batch sorption tests. We screened and identified suitable sorbents that have a higher capacity for selective removal of Cs from Ohaaki brines in acidic and basic environments. The cobalt-containing Prussian Blue (Co-PB) tested using 5 ppm Cs with and without competing sodium (Na) ions exhibited the overall best performance toward Cs adsorption capacity reaching as high as 31.6 g/kg and 19.0 g/kg in the presence of competing Na ions. The Co-PB was subjected to repeated adsorption, stripping, and regeneration cycles to assess any degradation in sorbent capacity. We also conducted Cs desorption and Co-PB regeneration experiments using different stripping agents (nitric acid and potassium chloride) to determine which stripping agent is ideal. The techno-economic analysis revealed that the internal return rate (IRR) for extracting 90 percent of Cs from a geothermal brine containing 700 ppb of Cs using the magnetic nanoparticle adsorption technology was about 6.1 percent. The IRR will increase with a higher concentration of Cs and lower capital cost, and it is not sensitive to the adsorbent cost when the adsorbent can achieve a 6,000 h lifetime and higher than 99.9 percent magnetic retention rate.

Acknowledgments

We thank Mr. Jerry Mills, Mr. Bart Mills, and Dr. Peter B. McGrail at Moselle Technologies and Mr. Jon Worth at Geo40 for their suggestions, guidance, and support. We also thank Dr. Alexandra Prisjatschew and Jeff Winick at the DOE Geothermal Technologies Office for her support and suggestions. Finally, we thank PNNL management for their support particularly Dr. Allan Tuan.

Acronyms and Abbreviations

AMP	ammonium molybdophosphate
BET	Brunauer-Emmett-Teller
CAPEX	capital cost
CFS	coagulation–flocculation–sedimentation
Co-PB	cobalt-based Prussian Blue analog ($Co_3[Co(CN)_6]_2$)
EPA	U.S. Environmental Protection Agency
FC	ferric chloride
Fe-PB	iron-based Prussian Blue analog ($Fe_4[Fe(CN)_6]_3$)
FOB	Free on Board
DOE	Department of Energy
HCl	hydrogen chloride
ICP	inductively coupled plasma
ICP-MS	inductively coupled plasma mass spectrometry
ICP-OES	inductively coupled plasma optical emission spectroscopy
IRR	internal return rate
MCL	maximum contaminant level
MOF	metal-organic framework
NPV	net present value
OPEX	operating cost
PB	Prussian Blue
PSD	pore size distribution
PXRD	powder x-ray diffraction
REE	rare earth element
RO	reverse osmosis
SRB	sulfate-reducing bacteria
sRF	spherical resorcinol-formaldehyde resin
XRD	x-ray diffraction

Contents

Figures

Tables

1.0 Introduction

Pacific Northwest National Laboratory (PNNL) with support from the Department of Energy's (DOE's) Geothermal Technologies Office has developed a simple and cost-effective nanofluid method for extraction of rare earth elements (REEs) from geothermal brine solutions (Elsaidi et al. 2018). Functionalized iron oxide-based core shell nanoparticles with high concentrations of chelating sites were used to selectively capture and separate REEs from geothermal brine solutions. Use of nanoparticles containing a high density of functional chelating groups enabled the easy separation of REEs and did not require any use of an expensive packed bed or membrane system—a bottle neck in large-scale REE separation. After a short residence time in contact with geothermal brines, the particles are effectively separated out with an applied magnetic field and standard extraction methods to strip the rare earth metals from the nanoparticles, which are then recycled back to the geothermal plant (**Error! Reference source not found.**). The sorbents developed by PNNL exhibited about >99.9 percent removal efficiency relative to REEs even after 2,000 cycles which PNNL commercialized this technology to Moselle Technologies LLC.

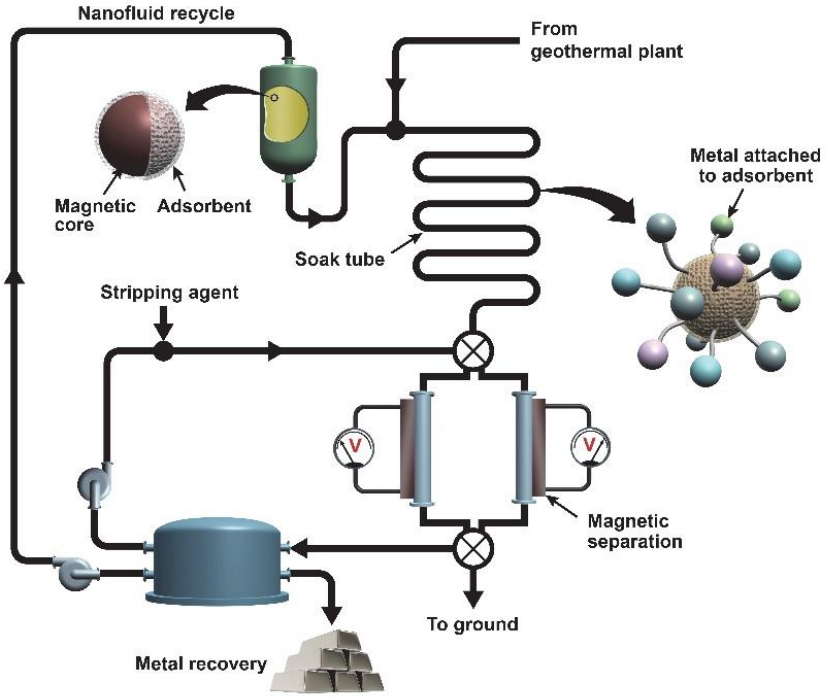

Figure 1. Illustration of the magnetic partitioning nanofluid extraction system.

Our industrial partner (Geo40) recently identified two elements, cesium (Cs) and antimony (Sb), that are present in Ohaaki brines at parts per million level amounts and could be sold to known customers if they could be produced at attractive prices. Therefore, PNNL, in collaboration with Moselle Technologies and Geo40 extended the magnetic separation technology to extract Cs selectively from geothermal brine by developing novel Cs-selective sorbent materials as a shell.

2.0 Sorbents for Selective Cesium Removal

In support of the DOE Office of Environmental Management, PNNL evaluated a large number of materials for Cs removal from Hanford tank waste. Some of the sorbents evaluated included ion exchange resins (Diphonix-CS) (Chiarizia et al. 1998), ammonium molybdophosphate (AMP) incorporated in a polyacrylonitrile (AMP-PAN) support (Campbell, Fiskum, and Peterson 2021), and various solvent extraction methods for selective removal of Cs from Hanford wastes. However, these materials exhibited lower selectivity and capacity toward Cs in the presence of other competing cations found in Hanford tank waste. On the other hand, two commercially available resin materials—spherical resorcinol-formaldehyde resin (sRF) (Brown 2014) and Dibenzo-18-crown-6 (D18C6) ethers—were found to outperform other sorbents for Cs removal from Hanford tank waste. For example, sRF was studied for extraction of Cs from higher alkaline conditions (pH 14) due to the presence of two weakly acidic hydroxyl groups on the resorcinol ring, which are deprotonated and eventually bind to Cs selectively. By switching the pH (say pH ~2) the adsorbed Cs can be removed from the sRF. Likewise, D18C6 was shown to have Cs selectivity at low pH (~7) due to the ideal pore size of D18C6, but no data exist for any of these sorbents about the efficacy of Cs removal from Ohaaki geothermal brine and its selectivity in the presence of other competing ions.

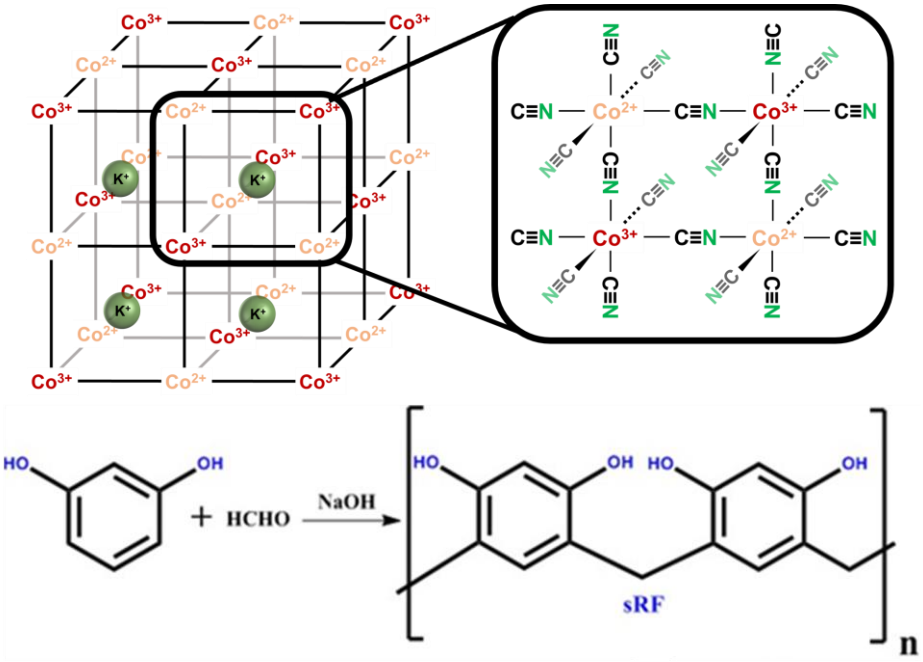

Figure 2. Sorbents studies for Cs uptake under conditions relevant geothermal brines, Co-PB (top) and sRF (bottom).

Therefore, we have successfully identified and developed Cs-selective sorbent materials that work under conditions relevant to geothermal brine solution. Several factors were taken into consideration to screen the sorbent materials, including (1) aqueous stability; (2) high Cs adsorption capacity and selectivity in the presence of competing ions, such as sodium (Na^+), potassium (K^+), magnesium (Mg^{2+}), etc.; (3) resistance to most chemicals including acids and bases; (4) synthetic tunability and cycle stability; and (5) large-scale production, if necessary. With these criteria in mind, we identified aluminosilicate clays including kaolinite and montmorillonite, because of their high surface area, capacity, and commercial availability. Likewise, Prussian Blue analogs (PBs) were also evaluated for Cs adsorption capacity, cycle stability due to its synthetic tunability, and ion exchange ability of PBs toward Cs. The PB

consists of cubic lattices where M^{2+} and M^{3+} are connected by cyanide groups to form a rigid network structure where alkali metal cations like Na^+ or K^+ are occupied in the pore space. The size of these channels (0.32 nm) is consistent with the hydrated radius of the Cs^+ ion (0.329 nm) (Faustino et al. 2008). Though a significant amount of literature exists about these sorbents for Cs removal, no data on the applicability of these materials under natural geothermal brine solutions exist. We evaluated these materials for Cs adsorption and desorption under Ohaaki brine conditions at room temperature.

2.1 Materials and Methods

All sorbents including dibenzo-18-crown-6 (D18C6), kaolinite, and montmorillonite, were obtained from commercial sources (Aldrich) and were used without any modification. The cobalt PB (Co-PB) and iron-based PB (Fe-PB) were synthesized according to the reported literature (Thallapally et al. 2010).

2.2 Cesium Extraction Experiments

To determine the amount of Cs absorbed, batch experiments were performed at room temperature using 5 ppm cesium solution. The 5 ppm Cs solution was prepared by dissolving a known amount of cesium nitrate ($CsNO_3$) in deionized water with and without 2M sodium chloride (NaCl) (pH ~5-6). A known amount of sorbent was added to 30 mL of Cs solution and allowed to stay undisturbed for a period of 24 h. After 24 h, the materials were removed from the solution by centrifugation, and the supernatant solution was analyzed using inductively coupled plasma mass spectrometry (ICP-MS) to calculate the Cs capacity. The Cs capacity of each sorbent at different pHs were determined by analyzing the supernatant solution using ICP-MS. The amounts of Cs adsorbed were calculated as follows:

$$Q = \frac{(C_0 - C_f) \times V}{m} \quad (1)$$

where

- Q = the adsorption capacity in g/Kg,
- C_0 = the initial concentration in mg/L (ppm),
- C_f = the equilibrium concentration after sorbent treatment in mg/L (ppm),
- V = the volume of the solution in liters, and
- m = the mass of the sorbent in grams.

Table 1 shows the Cs adsorption capacities of various sorbents using a 5 ppm Cs solution under a neutral condition (pH ~5-6) with and without NaCl (2M). As shown in Table 1, among all the sorbents tested the Co-PB exhibited high Cs adsorption capacity using 5 ppm Cs solution without NaCl, reaching as high as 31.6 g/kg. The Fe-PB exhibited the Cs capacity of 14.3 g/kg under the same conditions. On the other hand, the Co-PB showed a slight decrease in Cs capacity in the presence of Na ions but still demonstrated a very high Cs capacity of 19 g/kg. Similarly, the Fe-PB exhibited a slightly decreased Cs capacity of 8.3 g/kg. Other sorbents including sRF, D18C6, and clays show very marginal capacities under identical conditions.

Table 1. Cs adsorption capacity in various sorbents tested using 5 ppm Cs solution with and without 2M NaCl.

Sorbent	Cs Uptake Without NaCl (g/kg)	Cs Uptake in the Presence of 2M NaCl (g/kg)
D18C6	0.042	0.03
Kaolinite	0.491	0.514
Montmorillonite	1.074	0.149
sRF	0.552	0.606
Co-PB	31.62	19.002
Fe-PB	14.28	8.176

2.3 Prussian Blue: Effective Sorbent for Cesium Removal from Brines

Given the exceptional performance of PBs under neutral conditions (with and without NaCl), the PB sorbents were further evaluated at different pHs by adjusting 5 ppm Cs solution (with and without NaCl) using 1.0 M hydrogen chloride (HCl, pH ~2) and 1.0 M potassium hydroxide (KOH, pH ~8), respectively. As shown in Figure 3(a), the Co-PB adsorbs 31.6 g/kg of Cs under neutral conditions but exhibits a 10 percent reduction in Cs adsorption capacity under acidic conditions (27.3 g/kg) and 10 percent greater adsorption capacity under basic conditions (35.4 g/kg). On the other hand, pristine Fe-PB had about 14.2 g/ kg of Cs adsorption capacity under neutral conditions but a significant reduction in Cs adsorption capacity under acidic conditions (4.2 g/kg) compared to neutral and basic conditions (16.9 g/kg). When comparing Co-PB and Fe-PB, the Fe-PB has significant reduction in Cs adsorption capacity under acidic conditions, which could be due to the degradation of the Fe-PB; however, both Co-PB and Fe-PB perform well under neutral and basic conditions. Of these two sorbents, Co-PB outperforms Fe-PB in terms of Cs adsorption capacity exhibiting a more than 50 percent increase in Cs adsorption under all the tested conditions. Similar experiments were performed using 5 ppm Cs solution and 2M NaCl solution, adjusting the pH as described previously. These experiments will provide direct insight into the role of competing Na^+ and K^+ ions in solution under neutral, acidic, and basic conditions. As shown in Figure 3b, the Cs adsorption capacity in Co-PB is in the range of 18–21 g/kg under three different conditions (pH = 2, 6, and 8) in presence of competing Na, K ions, but the Cs adsorption capacity of Co-PB is significantly lower compared to when no competing Na ions were present (Figure 3a). Though the Co-PB exhibits a significant reduction in Cs adsorption capacity when competing Na, and K ions were present, the capacity is still higher than other sorbents. A similar trend was observed with Fe-PB when tested using 5 ppm Cs solution with 2M NaCl at different pHs. As described previously, the Fe-PB shows significantly lower Cs uptake under acidic conditions than the Co-PB. In general, the decrease in Cs adsorption capacity of Fe-PB under acidic conditions can be attributed to competitive adsorption of Cs ions that have large quantities of H^+ ions (Yang et al. 2018) and the possibility of structural degradation (Loos-Neskovic et al. 2004) compared to Co-PB. The higher adsorption capacity of Co-PB could be due to its higher specific Brunauer-Emmett-Teller (BET) surface area compared to Fe-PB (see below).

Based on these batch experiments, Co-PB is a promising adsorbent for Cs compared to Fe-PB. This finding resulted in further studies pertaining to repeated adsorption, Cs stripping (desorption), and regeneration cycles to assess the overall suitability of Co-PB for Cs removal.

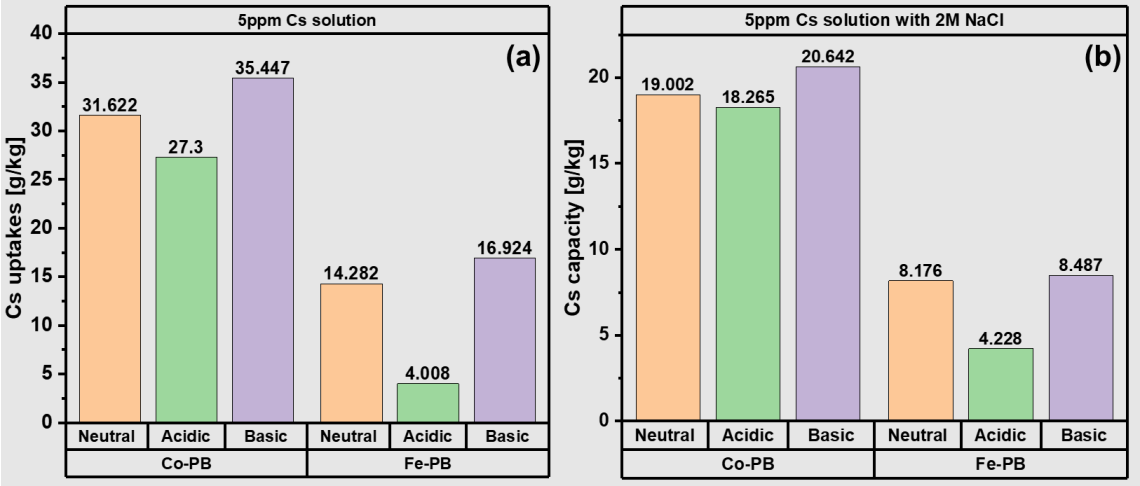

Figure 3. Cs adsorption capacities of Co- and Fe-PB in 5 ppm Cs solution under neutral, acidic, and basic conditions (a) and 5 ppm Cs solution (in the presence of 2M NaCl) with neutral, acidic, and basic conditions (b), respectively.

To understand the reduced Cs adsorption capacity under acidic conditions, the supernatant solutions after Cs adsorption were analyzed using inductively coupled plasma optical emission spectroscopy (ICP-OES) to monitor the concentration of elemental Co and Fe, if any, due to dissolution of Co- and Fe-PBs in aqueous media. Our results showed that Co-PB maintained a constant Co ion concentration under all conditions (neutral, acidic, and basic), while the Fe concentration in Fe-PB samples increased under acidic conditions, suggesting partial or complete dissolution of Fe-PB in acidic environments. The small amount of Co and Fe detection under all pH conditions is well within the acceptable limits. Table 2 illustrates the Co and Fe ion concentrations obtained from the ICP-OES analysis of the supernatants after the Cs adsorption experiment.

Table 2. The concentrations of Co and Fe in supernatant solutions after batch experiments with Co- and Fe-PB using 5 ppm Cs solution (with 2M NaCl) under neutral, acidic, and basic conditions.

Sample[(a)]	Na (wt%)	Co (ppm)	Fe (ppm)
Cs and NaCl stock solution (N)	4.25	< 1	< 1
Cs and NaCl stock solution (A)	4.25	< 1	< 1
Cs and NaCl stock solution (B)	4.08	< 1	< 1
Co-PB (N)	4.18	5.41	Not detected
Co-PB (A)	4.15	5.27	Not detected
Co-PB (B)	4.12	5.29	Not detected
Fe-PB (N)	4.29	Not detected	2.14
Fe-PB (A)	4.23	Not detected	5.16
Fe-PB (B)	4.29	Not detected	2.84

(a) N = In neutral environment (pH = 5.5).

A = In acidic environment (pH = 2).
B = In basic environment (pH = 8-8.5).

Similar experiments were performed to understand the aqueous stability of Co- and Fe-PB (without 2M NaCl) in acidic, basic, and neutral media by soaking these sorbents for 24 h and measuring the concentration of Co and Fe ions in supernatants (Table 3). Our results show that Fe-PB released a large amount of Fe ions under acidic conditions, which is three times higher than the amount of Fe ions released under neutral and basic conditions. This suggests that Fe-PB is structurally unstable under acidic conditions and may have experienced partial collapse of the structure.

Table 3. The concentrations of Co, and Fe in supernatant solutions after batch experiments with Co- and Fe-PB using 5 ppm Cs solution (without Cs and NaCl) under neutral, acidic, and basic conditions.

Sample[(a)]	Co (ppm)	Fe (ppm)
Stock solution (N)	< 1	< 1
Stock solution (A)	< 1	< 1
Stock solution (B)	< 1	< 1
Co-PB (N)	13.1	Not detected
Co-PB (A)	11.9	Not detected
Co-PB (B)	12.3	Not detected
Fe-PB (N)	Not detected	9.67
Fe-PB (A)	Not detected	27.0
Fe-PB (B)	Not detected	9.80

(a) N = In neutral environment (pH = 5.5).
A = In acidic environment (pH = 2).
B = In basic environment (pH = 8-8.5).

To continue to evaluate the origins of lower Cs capacity under acidic conditions, powder x-ray diffraction (PXRD) and BET analyses were performed to assess the structural integrity and porosity of Co- and Fe-PB before and after adsorption experiments. Figure 4 illustrates the PXRD patterns of Co- and Fe-PBs after Cs adsorption in the presence of NaCl under neutral (N), acidic (A), and basic (B) conditions. The PXRD patterns of the pristine Co- and Fe-PB are provided for comparison. Both Co- and Fe-PB maintained their crystal structures after adsorption under various conditions. Specifically, the PXRD results for Fe-PB indicate the structural integrity was preserved throughout the experiment, except that the peak intensity of Fe-PB was slightly reduced under acidic conditions despite increased Fe concentration in the acidic environment based on the ICP-OES measurements. The combination of the ICP and PXRD results suggest Co-PB is robust under all the conditions tested. Similarly, Fe-PB was shown to retain its structure, but the presence of increased Fe concentrations suggests partial dissolution of Fe without compromising its structural integrity; however, prolonged exposure of Fe-PB to aqueous solution might result in complete degradation of Fe-PB (needed further evaluation).

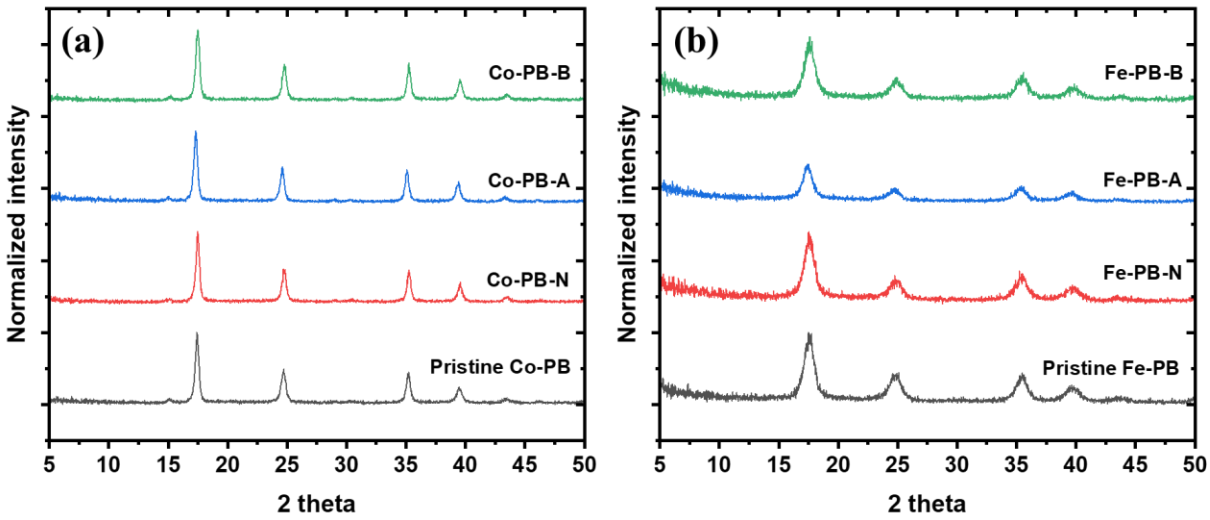

Figure 4. The XRD patterns of Co-PB (a) and Fe-PB (b) after being exposed to 5 ppm Cs solution (with 2M NaCl) under neutral (N), acidic (A), and basic (B) conditions.

With these results on hand, we then focused our attention on examining the surface area of the PBs. Surface area measurements confirmed that both PBs maintained porosity before and after Cs adsorption (Figure 5). To measure the BET surface area of the Cs-loaded PBs were washed with fresh deionized water three times and then activated at 100°C overnight and nitrogen (N_2) adsorption/desorption isotherms at 77 K were performed. The Co-PB shows similar BET surface areas (788 m^2/g) compared to pristine Co-PB (841 m^2/g). The Fe-PB showed a BET surface area (168 m^2/g vs. 188 m^2/g for pristine PB). The surface area results are consistent with PXRD, suggesting Co- and Fe-PB materials maintained their porosity after the batch Cs adsorption experiment using 5 ppm Cs with 2M NaCl solution under neutral, acidic, and basic conditions. The reduced Cs uptake in acidic solution by Fe-PB could be due to the reduced surface area compared to Co-PB, which is confirmed from our surface area experiments.

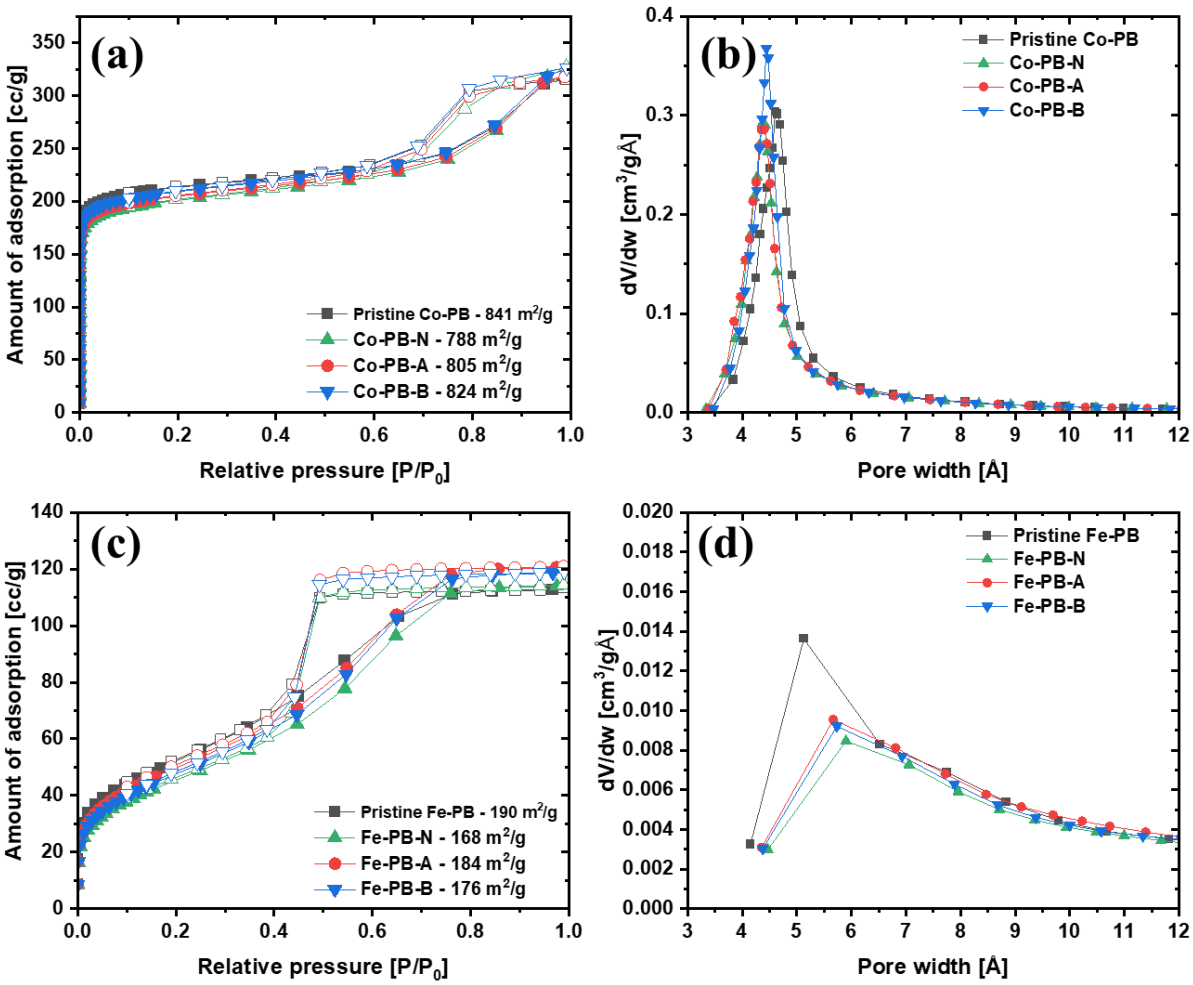

Figure 5. BET surface area and pore size distribution of Co-PBs (a and b) and Fe-PB (c and d) before and after Cs adsorption experiments under neutral (N), acidic (A), and basic (B) conditions.

Given the structural stability and exceptional Cs adsorption capacity of PBs, experiments were focused on recycling the sorbent material under different conditions. In the first experiment, Cs-loaded PBs were soaked in 30 mL of 2M nitric acid (HNO_3) for 2, 14, and 24 h. In the second experiment Cs-loaded PBs were soaked with 4M potassium chloride (KCl) solution for the same amount of time. The solutions containing PBs were filtered and the concentrations of Cs in the supernatants were measured using ICP-MS. As shown in Figure 6a and c, around 13 percent of adsorbed Cs was desorbed when the sorbent was washed with 2M HNO_3, while 23 percent was desorbed when 4M KCl was used from Co-PBs. Interestingly, the Cs desorption from Co-PB using 2M HNO_3 remained constant regardless of the desorption time and same is true with 4M KCl solution. On the other hand, the amount of Cs desorbed from Fe-PB increased with time when washed with 2M HNO_3 (9.59 percent at 2 h vs. 15.8 percent at 24 h, Figure 6b), whereas the amount of Cs desorbed from Fe-PB with 4M KCl was same, irrespective of the time. Our Cs regeneration experiments suggest the Cs recovery from Co-PBs was higher when washed with KCl than with HNO_3; however, more experiments are needed to evaluate the complete recovery of Cs from these sorbents' materials.

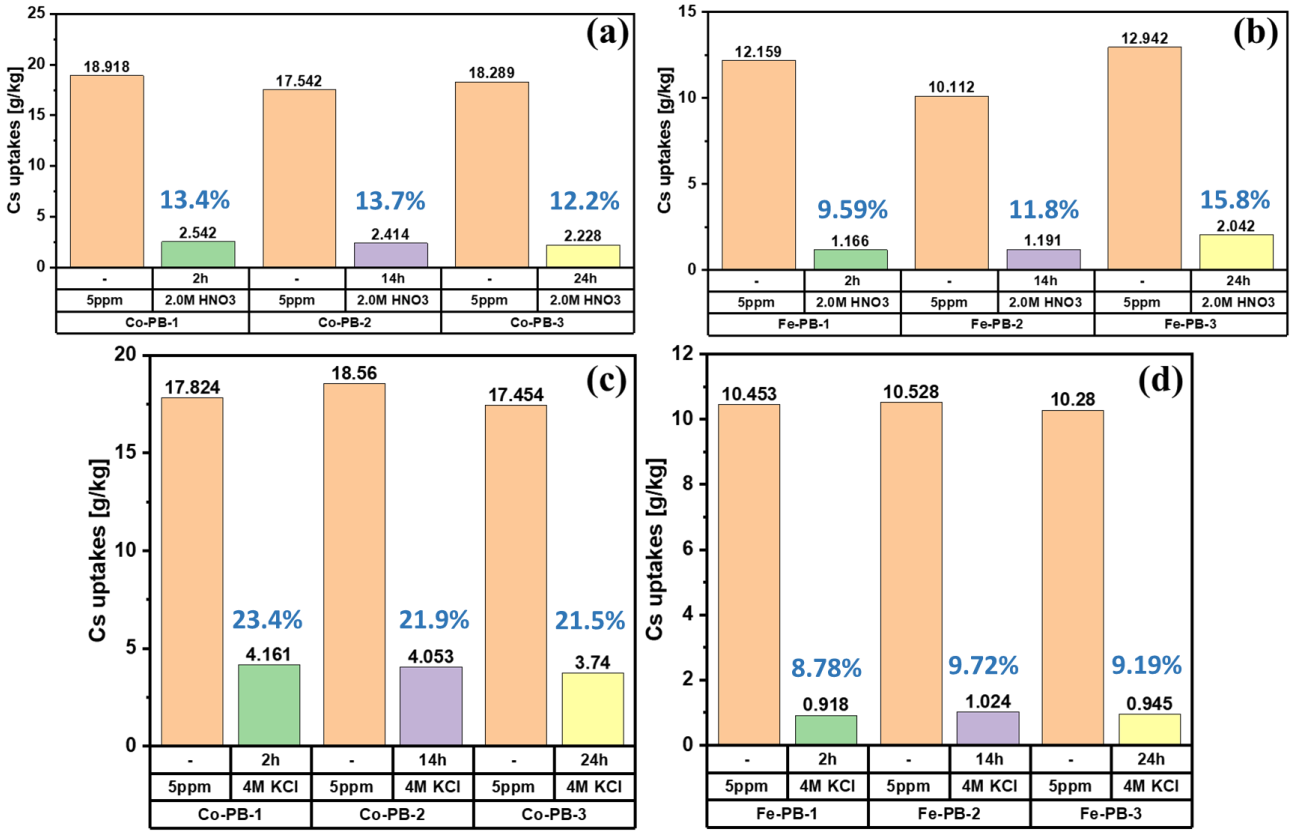

Figure 6. The recyclability of Co- and Fe-PBs from Cs-loaded PBs using 2M HNO_3 (a and b) and 4M KCl solution (c and d) as a function of time.

Given the exceptional Cs adsorption capacity of Co-PB under various conditions, batch experiments were conducted to investigate the Cs adsorption from two different natural geothermal brines that we received from our industrial client (Geo40). The geothermal brine labeled as Geo40 contains 0.76 ppm Cs with a pH close to 8.24 and the second brine labeled as Geo-40-NP contains 0.744 ppm Cs with a pH of 1.98. Table 4 illustrates the Cs uptake using Co- and Fe- PB from two different Ohaaki brines at room temperature. Of the two PB analogs, the Co-PB exhibits higher Cs adsorption capacity (0.42 g/kg) in Geo-40-NP with almost a 98.31 percent Cs removal efficiency compared to Ohaaki brine Geo-40 at pH 8.24 (0.34 g/kg), which exhibits about a 95.1 percent cesium removal efficiency. These results are quite promising in terms of Cs extraction from Ohaaki brines using PB analogs.

Table 4. Cesium uptake capacity of Co- and Fe-PB analogs using two different Ohaaki brines (Geo-40) and (Geo-40-NP) at room temperature.

Sample	pH	Cs Capacity (g/kg)	Cs Removal (%)
Co-PB-Geo-40	8.24	0.342	95.12
Co-PB-Geo-40-NP	1.98	0.419	98.31
Fe-PB-Geo-40	8.24	0.239	93.57
Fe-PB-Geo-40-NP	1.98	0.143	55.63

2.4 Cesium Removal Using sRF

As for PB, we conducted a more detailed investigation using sRF, which has proven to be an effective sorbent for Cs extraction from highly alkaline media, which can be attributed to the presence of –OH group, which ionizes under high alkaline condition. The sRF demonstrated a Cs adsorption capacity of 0.552 g/kg under neutral conditions using 5 ppm Cs solution (Table 5). Although sRF has a lower Cs adsorption capacity under neutral pH conditions, it is known to be an extremely selective sorbent for Cs at higher pH levels. To further confirm the Cs adsorption capacity using sRF under different pH conditions, we evaluated the Cs adsorption capacity under neutral, acidic, and basic conditions by adjusting 5 ppm Cs solution with HCl and KOH to achieve the desired pH (Table 5 and Figure 7a). The Cs adsorption capacity of sRF was found to be 0.522 g/kg under neutral conditions, 0.163 g/kg at pH 2 and 0.778 g/kg at pH 8-8.5. In comparison, Co- and Fe- PBs outperform Cs adsorption capacity under identical conditions at all tested pH ranges (Figure 3).

Table 5. Cs loading in sRF at room temperature using 5 ppm Cs solution at different pHs.

Sample[(a)]	pH	Cs Capacity (g/kg)	Cs Removal (%)
sRF	5.4	0.552	36.40
sRF-A	2	0.163	10.48
sRF-B	8-8.5	0.778	47.52

(a) A = In acidic environment (pH = 2).
B = In basic environment (pH = 8-8.5).

Next, we investigated the regeneration of sRF using different concentrations of HCl. The sRF was immersed in 5 ppm Cs solution with 2M NaCl under neutral conditions for 24 h. The Cs-loaded sRF was soaked in a solution containing 0.1, 0.3, 0.5, and 1.0M HCl solutions for 1 and 24 h, respectively. As shown in Figure 7b and c, the Cs regeneration capacities of sRF increased with increasing HCl concentrations. Notably, 1M HCl exhibited the Cs regeneration efficiency of 17.8 percent, which was significantly higher than that of 0.1M HCl. Additionally, sRF exhibited higher Cs regeneration when soaked in HCl for 24 h under the same conditions. In particular, the regeneration using 1M HCl resulted in efficiency of 75.7 percent, suggesting that the high concentration HCl solution facilitates desorption of the Cs^+ ion from Cs-loaded sRF.

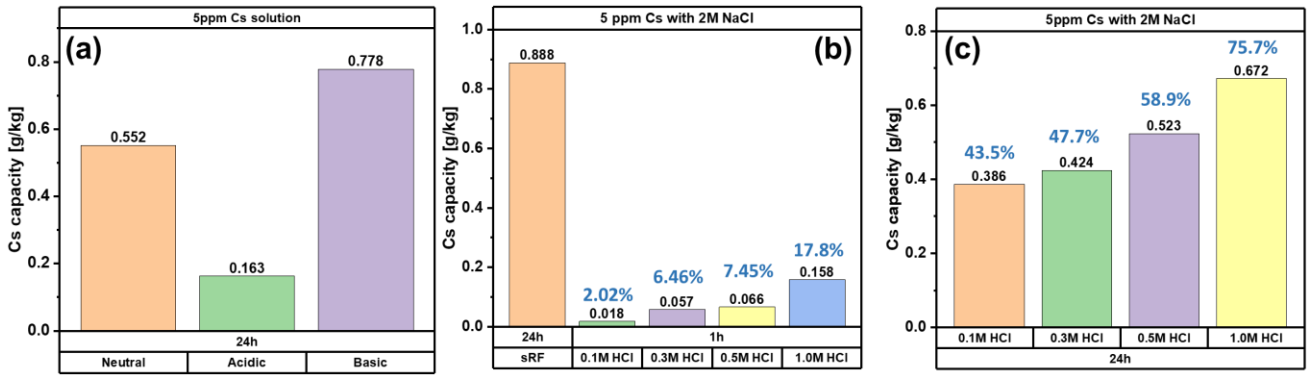

Figure 7. (a) Cs capacities of sRF in 5 ppm Cs solution under neutral (pH = 5.5), acidic (pH = 2), and basic (pH = 8-8.5) conditions; the Cs regeneration of sRF for (b) 1 h and (c) 24 h using various HCl concentration solutions.

We also evaluated the effectiveness of sRF for Cs extraction from natural brine solutions (Geo40 and Geo40-NP) provided by our industrial partner. As shown in Figure 8a, the Cs adsorption capacity of sRF in Geo40-NP was significantly reduced due to the acidic environment, which is consistent with our previous test results. The sRF exhibited a modest Cs adsorption capacity of 0.167 g/kg in Geo40—significantly lower than Co-PB that we tested (Table 4). The Cs regeneration experiments were also performed using Cs-loaded sRF using 0.3, 0.5, and 1M HNO_3 solution (Figure 8b). After 2 h, the 1M HNO_3 solution exhibited a Cs regeneration efficiency of 55.5 percent, indicating that Cs extracted from Geo40 using sRF can be easily regenerated using 1.0 M HNO_3 solution compared to the 1M HCl solution.

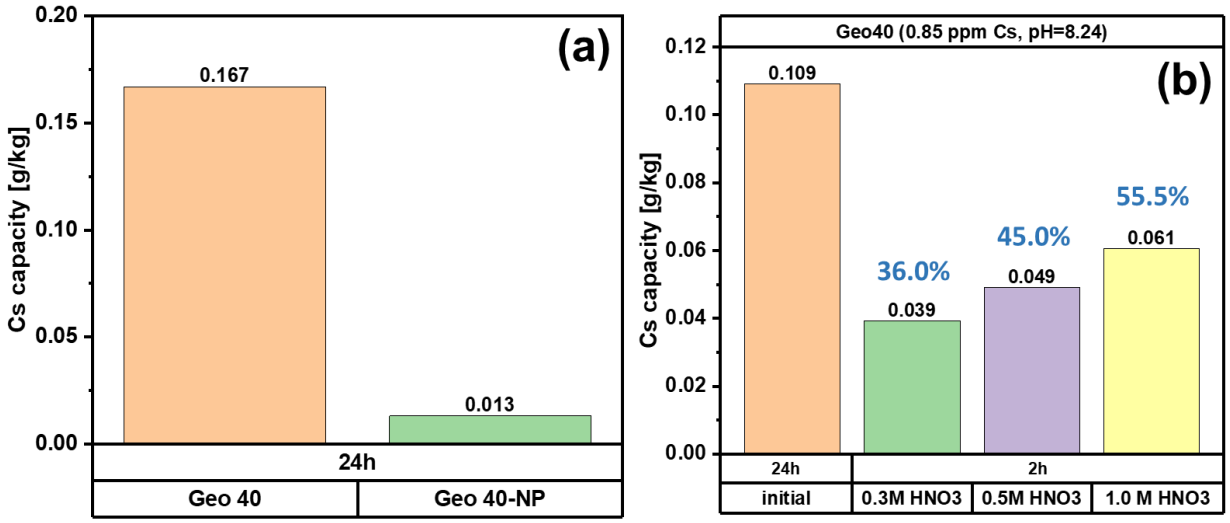

Figure 8. Cesium uptake in sRF from Geo40 (pH = 8.24) and Geo40-NP (pH = 1.9) brine solution (a) and Cs regeneration from Cs-loaded sRF using 0.3, 0.5, and 1M nitric acid solution.

3.0 Preliminary Techno-Economic Analysis

The goal of the preliminary techno-economic analysis is to evaluate the internal return rate (IRR) of the investment for using the magnetic nanoparticle adsorption technology to extract Cs from geothermal brine. Capital cost (CAPEX) and operating cost (OPEX) were estimated based on the adsorption performance, literature data, vendor price, and assumed process information, and the IRR was calculated based on these inputs and financial assumptions used by the DOE Geothermal Technologies Office.

3.1 Adsorbent Cost and Value Estimation

The nanoparticle adsorbent concentration for a particular sample with a known equivalent diameter and surface area can be calculated based on the metal ion removal rate using a plug-flow reactor model, as shown in Figure 9 and described in our previous study (J. Liu, Martin, and McGrail 2022). A key assumption is that an excess number of complexation sites exists on the particle surfaces so that molecular collisions with those sites result in a nearly constant rate of removal from the brine, as was assumed in the plug-flow reactor model. Using the Cs adsorption working capacity obtained for the Co-PB adsorbent (shown in Figure 6c) and assuming an active site area and other common parameters as similar to those used in the previous study, the concentration of the nanoparticle adsorbent was estimated to be at least 0.3 wt%. To achieve a 90 percent removal rate of Cs from the solution, the mass of nanoparticle adsorbent Co-PB required to extract Cs from a geothermal brine with a flow rate of 6,800 gallon/min was estimated to be 52.2 kg using the equation shown in Figure 9.

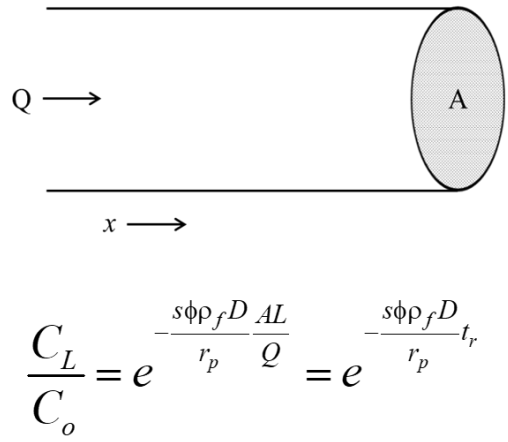

Parameters			Removal Efficiency	Nanoparticle Mass (kg)
Q (gal/min)	6800		80%	36.5
s (cm^2/g)	5.35×10^6		90%	52.2
ϕ	0.3%		99%	104.5
ρ_f (g/cm^3)	1.1			
D (cm^2/s)	3×10^{-6}			
t_r (s)	20			
r_p (cm)	4.25×10^{-5}			

Figure 9. The plug-flow reactor model and the parameters used to estimate the loading of adsorbent particles.

The cost of the adsorbent was estimated to be about $107.6/kg as shown below using a formula like that in our previous work. The cost of the Fe_3O_4@Co-PBis much less than that of the core shell metal-organic frameworks (MOFs) used in the case of REEs (Jian Liu, Martin, and McGrail 2021).

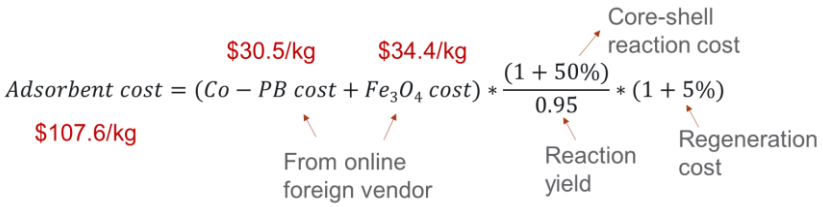

$$Adsorbent\ cost = (Co - PB\ cost + Fe_3O_4\ cost) * \frac{(1 + 50\%)}{0.95} * (1 + 5\%)$$

The price for the Cs metal (99.5 percent) was estimated to be $162/kg from the average FOB China price of Cs_2CO_3 in 2023. The productivity of the Cs depends on the concentration of Cs and the recovery rate, which is set to 90 percent by default.

3.2 Installed Equipment Cost

The CAPEX will be estimated based on the installed equipment cost, which will be estimated using Aspen Plus Economic Analyzer and process information such as flow rates. The cost of the electromagnet was estimated from the information provided by the vendor on a smaller system. The total equipment purchased cost was estimated to be around $3.3 M (2018 US dollar). The average installation factor was assumed to be 1.2 and the installed equipment cost was converted from 2018 US dollars to 2022 US dollars—$5.5 M.

Table 6. Estimated cost of the purchased equipment.

Code	Equipment	Type	Size or rate	Material	Units cost	Number of unit	Sum. Cost in 2018
51	Soaking tubes	Pipe	24 inch O.D. 100 ft	Fiberglass	$155/ft + $703/elbow	100 ft	$ 27,707
12	Centrifugal pump for nanofluid injection	Pump	0.1 L/s with 12 m head	316 Stainless steel	$2,865	1	$ 2,865
13	Centrifugal pump for stripping fluid	Pump	2 L/s with 12 m head	316 Stainless steel	$2,628	1	$ 2,628
11	Centrifugal pump for nanofluid recycle	Pump	0.1 L/s with 12 m head	316 Stainless steel	$2,865	1	$ 2,865
61	Stir tank for nanofluid	Tank	40 Gallon Ace Roto Mold Full Drain Inductor Tank	Polyethylene with PTFE coating	$562	1	$ 562
64	Stir tank for $NaHCO_3$ mixing	Tank	40 Gallon Ace Roto Mold Full Drain Inductor Tank	Polyethylene with PTFE coating	$562	1	$ 562
62	Tank for stripping fluid	Tank	300 Gallon 45 Degree Cone Bottom Tank	Polyethylene	$909	1	$ 909
63	Stir tank for desorption	Tank	150 Gallon 45 Degree Cone Bottom Tank	Polyethylene with PTFE coating	$1,024	1	$ 1,024
66	Tank for HCl make-up	Tank	100 Gallon Cone Bottom Batch Tank	Polyethylene	$507	1	$ 507
65	Tank for $NaHCO_3$ make-up	Tank	100 Gallon Cone Bottom Batch Tank	Polyethylene	$387	1	$ 387
23	Centrifugal separator for stripping	Separator	10 m^3/h disc stack centrifugal separator	Stainless steel	$3,600	1	$ 3,600
24	Centrifugal separator for $NaHCO_3$ washing	Separator	5 m^3/h disc stack centrifugal separator	Stainless steel	$1,200	1	$ 1,200
21,22	Magnetic separator	Magnet	Dipole Electromagnet 0.6T at 204 mm	Carbon steel, copper	$1,620,576	2	$ 3,241,151
	Magnetic separation tubes	Pipe	8 inch O.D. 300 ft	Fiberglass	$28.6/ft + $215/elbow	10 sets of 30 ft	$ 12,892
SV1-3	Major control valves	Valve	24 in Basic Control Valve CF Flanged 150#	Carbon steel	$23,428	3	$ 70,284
	Miscellaneous (tube, accessory)	Other	Various	Various	$3,000	1	$ 3,000
						Sum. Cost	**$ 3,372,142**

3.3 Internal Return Rate Estimation

The IRR is a metric used in financial analysis that accounts for the time value of money to estimate the profitability of potential investments. The IRR was calculated using a discounted cash flow analysis when the net present value (NPV) of all cash flows equals zero (Table 7). The IRR was calculated to be 6.1 percent based on a case where 90 percent of the 700 ppb Cs was recovered using the magnetic adsorbent technology.

Table 7. The estimated IRR based on the CAPEX, OPEX, and selected financial parameters.

Parameters				
FCI				$ 8,691,281
TCI				$ 11,037,927
Debt		45%		
Equity		55%		
Interest on debt		4.3%	Y2017	
Preferred dividend rate		0.00%		
Repayment term of debt		10	years	
Capital Expenditure Period		2	years	
completion in year	0	0%		
completion in year	1	30%		
completion in year	2	70%		
completion in year	3	0%		
completion in year	4	0%		
completion in year	5	0%		
Operation begins at year		3		
Operational Period		30	years	
Ramp Up Period				
capacity in year	3	100%		
capacity in year	4	100%		
capacity in year	5	100%		
Escalation of O&M, fuel, revs		3.00%		
Discount rate		10.00%		
Capital Cost Escalation prior to operation		0.397%		
Capital Depreciation period		20	years	
Depreciation X-declining balance		150%		
Corporate Tax Rate (fed+state)		38%		
Effective Annual Rate of Equity				
Cost of Capital				
Cost-Year Dollars		2022		
WACC		4.57%		
IRROE		**6.13%**		

3.4 Sensitivity Analysis

Sensitivity analysis determines how different values of an independent variable affect a particular dependent variable under some assumptions. In our study, the dependent variable is the IRR and the independent variables include, but are not limit to, the concentration of Cs, the removal efficiency of Cs, the installed equipment cost, and the adsorbent cost. As mentioned earlier, the IRR was estimated to be 6.1 percent under the default condition. The IRR was recalculated in the sensitivity analysis case with a 10 percent decrease or increase in the dependent variable parameters. The relative change in the IRR is plotted in Figure 10. The IRR depends on the concentration and the removal efficiency of Cs in the geothermal brine solution. The reduction of the installed equipment cost, in other words, the reduction of electromagnet cost, can significantly boost the IRR. From our previous work, the adsorbent cost does not affect the IRR if reasonable lifetime (1,000 h) and magnetic retention rates (>99.9 percent) are met as discussed in our previous work (J. Liu, Martin, and McGrail 2022). Note that the flowsheet was not updated to accommodate much higher concentrations (e.g., 100 ppm). The process and

adsorbent were assumed to work for all the cases in the sensitivity analysis. It is likely that the IRR can be increased to 15 percent with higher concentrations of Cs and the less expensive option of using the magnet.

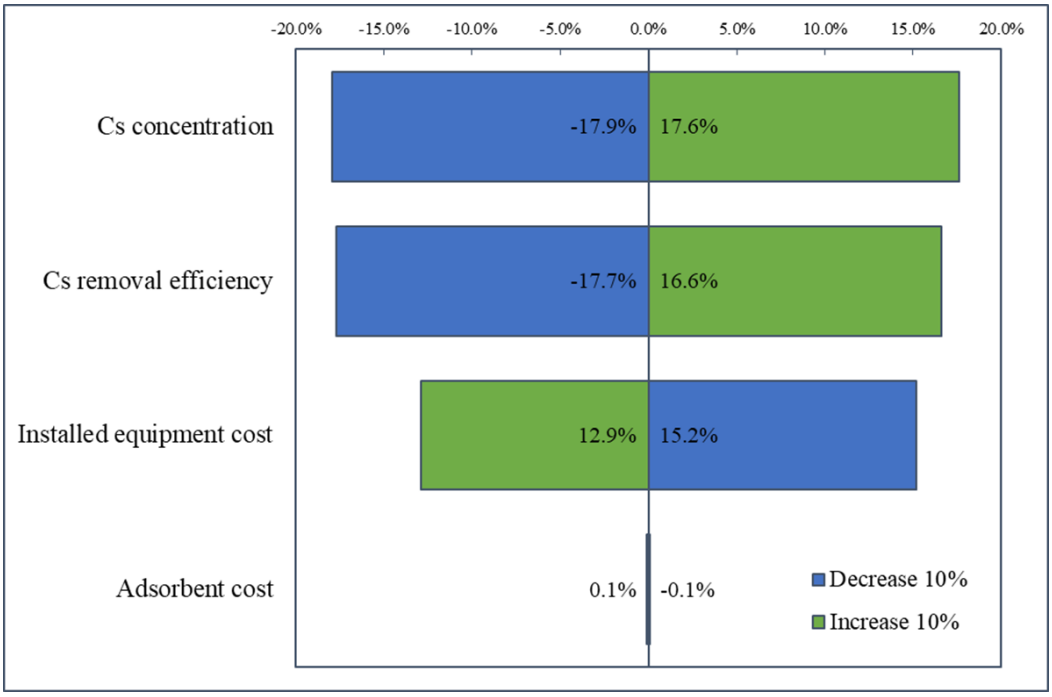

Figure 10. The relative change in the IRR.

4.0 Magnetic Core Shell Particle Development

Given the positive IRR results, we attempted to grow Co-PB analog around the magnetic core using the procedure reported in the literature. To synthesize the Fe_3O_4@Co-PB, we initially prepared Fe_3O_4 using a modified method described in the literature (Melo et al. 2013). Briefly, 0.1M anhydrous $FeCl_3$ (4.055 g) and 0.05M $FeCl_2{\cdot}4H_2O$ (2.485 g) were dissolved in 500 mL of deionized water that was stirred at room temperature. Then 1M NaOH aqueous solution was added to the mixed solution at room temperature until pH 12 was reached. Upon addition of NaOH, Fe_3O_4 nanoparticles were precipitated instantaneously. This precipitate was maintained at 45 ºC for 30 min with stirring under N_2 atmospheric conditions. The resulting Fe_3O_4 precipitates were separated from the supernatant using a magnet and washed with fresh water and acetone several times until the supernatant reached pH 6. The obtained Fe_3O_4 nanoparticles were dried at 100 ºC for 1 h. The Fe_3O_4@Co-PB core shell particles were developed using synthesized Fe_3O_4 nanoparticles (C. Carvalho et al. 2018). Around 0.5 g of Fe_3O_4 was dispersed in 250 mL of 5×10^{-5} M $K_3[Co(CN)_6]$ (0.415 g) with stirring at room temperature. Next, 250 mL of 9×10^{-5} M $Co(NO_3)_2{\cdot}6H_2O$ (0.653 g) aqueous solution was slowly dropped into the Fe_3O_4 and $K_3[Co(CN)_6]$ mixture and stirred for 12 h at room temperature under N_2 atmospheric conditions. The obtained brown-colored particles were washed with fresh water and acetone several times. The obtained dark brown particles were isolated from the acetone supernatant using a magnet and dried at 70 ºC overnight.

The PXRD patterns were performed to confirm the crystallinity of the synthesized Fe_3O_4@Co-PB. As shown Figure 11a, the XRD pattern of Fe_3O_4@Co-PB revealed the presence of two

distinct peaks: one corresponding to the Co-PB and the other is to the Fe_3O_4, suggesting successful synthesis of magnetic core shell particles. The BET surface area measurements confirm Fe_3O_4@Co-PB core particles exhibited significant porosity with a surface area of 267 m^2/g compared to pristine Co-PB (~ 840 m^2/g) and Fe_3O_4 (~ 110 m^2/g), indicating the successful coating of porous Co-PB on the Fe_3O_4 surface (Figure 11b).

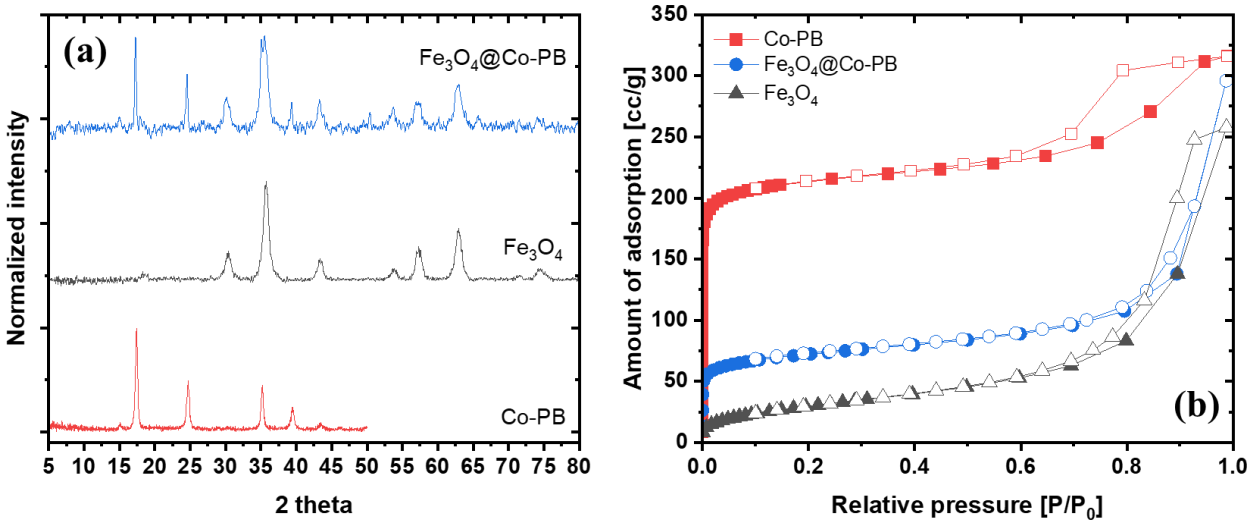

Figure 11. PXRD patterns of Fe_3O_4@Co-PB (a) and surface area measurements of Fe_3O_4@Co-PB, Co-PB and Fe_3O_4 (b).

Next, magnetic susceptibility testing was conducted using in-house capability; results showed the saturation magnetization of ~36 emu/g (Figure 12), which is lower than pristine Fe_3O_4 nanoparticle (~60 emu/g) at room temperature. This was expected because of the presence of the Co-PB shell around the magnetic core. Our previous experiments suggest saturation magnetization depends on the thickness of the shell. Our results show the core shell particles are magnetic even with the laboratory magnet shown in Figure 12.

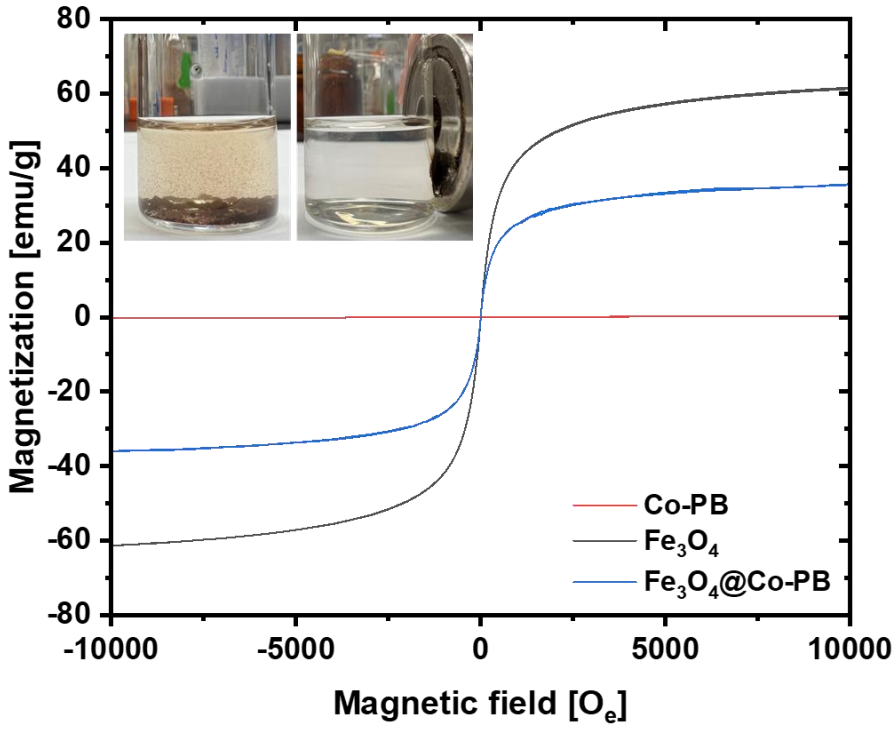

Figure 12. Magnetization as a function of applied magnetic field at RT of Co-PB, Fe_3O_4 and Fe_3O_4@Co-PB.

The Cs extraction experiments were performed on Fe_3O_4@Co-PB in the same way as the previous Cs extraction experiments. Briefly, ~5 mg of Fe_3O_4@Co-PB was soaked in 30 mL of 5 ppm Cs solution with 2M NaCl under neutral, acidic and basic conditions. The core shell particles were allowed to stay undisturbed for a period of 24 hours and removed from the solution using magnet. The collected supernatant solution was analyzed using ICP-MS to calculate the Cs capacity. Figure 13 presents the Cs extraction results on the core-shell Fe_3O_4@Co-PB under different pH conditions. Under neutral condition, the core-shell Fe_3O_4@Co-PB demonstrated a Cs adsorption capacity of 12.9 g/kg, which is approximately 30% lower than that of pristine Co-PB due to reduced surface area. Furthermore, the Fe_3O_4@Co-PB exhibited a 20-25% decrease in Cs capacity under both acidic and basic conditions compared to the neutral condition, resulting in capacities of 9.58 and 10.2, respectively. This decrease in Cs capacity under acidic condition aligns with the trend observed in Cs extraction experiments of pristine Co-PB, where competition with H+ ions can reduce the Cs adsorption capacity. However, the decrease in Cs adsorption under basic condition differs from the trend of pristine Co-PB. Pristine Co-PB showed a higher Cs capacity of 20.6 g/kg under basic condition compared to Cs capacity (19 g/kg) under neutral condition (see Figure 3b). In contrast, Fe_3O_4@Co-PB demonstrates a relatively low Cs adsorption capacity (10.2 g/kg) under basic condition compared to the Cs capacity (12.9 g/kg) under neutral condition. Further studies are needed to address this issue and gain a better understanding of the observations.

Additionally, to assess the structural stability of the core-shell Fe_3O_4@Co-PB, the dissolution of Co and Fe in the Cs aqueous medium was examined by analyzing the supernatant using ICP-OES after Cs adsorption under different pH conditions. The Fe_3O_4@Co-PB was exposed to neutral (pH = 5.5), acidic (pH = 2) and basic (pH = 8.5) conditions for a duration of 24 hours, and the concentrations of Co and Fe in the supernatant were measured. The results showed

that the concentrations of Co and Fe in the supernatant were both below 10 ppm, regardless of the pH values. This indicates that the Fe_3O_4@Co-PB retains its structural stability and does not undergo partial or complete dissolution in Cs aqueous solutions under both acidic and basic conditions.

Based on the structural stability of the core shell particles and its excellent Cs adsorption capacity, regeneration experiments were conducted. Previous regeneration experiments with pristine Co-PB demonstrated higher Cs recovery when washed with KCl solution compared to HNO_3. Therefore, the Cs-loaded Fe_3O_4@Co-PB was soaked with 4M KCl solution for 24 hours, and the supernatant solution was measured using ICP-MS. As shown in Figure 13b, approximately 32 percent of Cs was desorbed when the Cs-loaded Fe_3O_4@Co-PB was washed with 4M KCl. Interestingly, this represents a higher recovery rate compared to pristine Co-PB, which showed a recovery of 21% at 24 hours (see Figure 6c). These results suggest that Cs desorption using KCl solution is effective for Cs-loaded Fe_3O_4@Co-PB. However, further experiments are needed to evaluate the complete recovery of Cs from the core-shell Fe_3O_4@Co-PB.

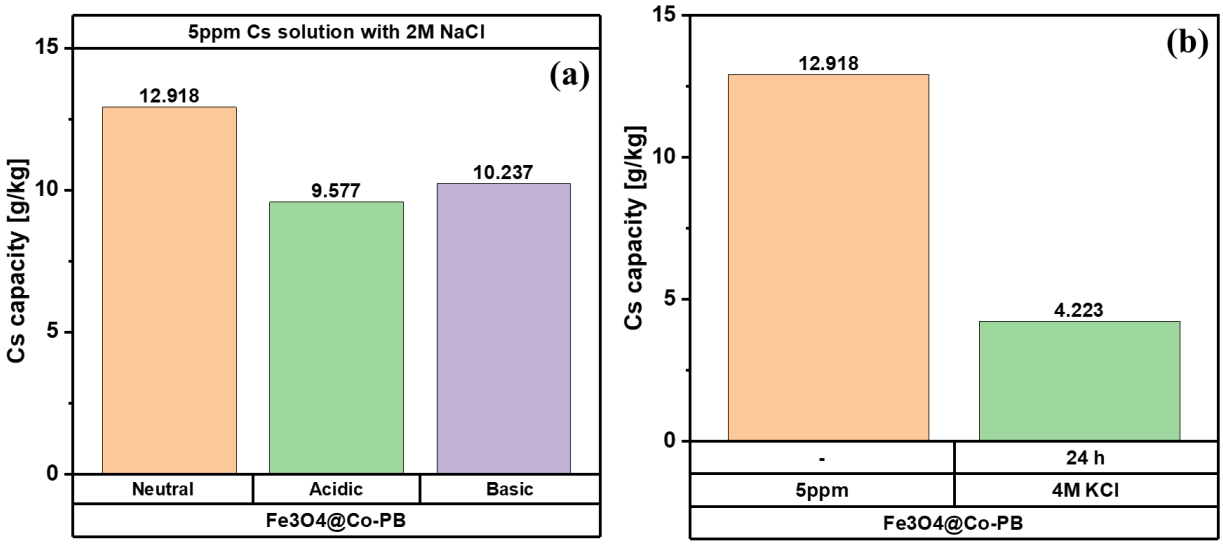

Figure 13. Cs adsorption capacities of Fe_3O_4@Co-PBs in 5 ppm Cs solution (in presence of 2M NaCl) under neutral, acidic, and basic conditions (a). he recyclability of Fe_3O_4@Co-PB using 4M KCl solution (b).

We also assessed the Cs removal efficiency from a natural brine solution provided by an industrial partner. As shown in Figure 14, Fe_3O_4@Co-PB demonstrated a high Cs capacity of 3.47 g/kg in Geo-40, indicating its effectiveness even very low Cs concentrations (0.75 ppm). On other hand, the Geo-40-NP tend show reduced Cs capacity due to acidic environment of the brine solution. Remarkably, when comparing these results to Table 4 (pristine Co-PB), the higher Cs capacity capacities were observed with Fe_3O_4@Co-PB. This is attributed to the difference in the amount of sorbents used for Cs extraction. In previous tests, ~100 mg of pristine Co-PB and Fe-PB were used for Cs extraction in Geo-40 and Geo-40-NP solutions. However, in Cs extraction experiments with Fe_3O_4@Co-PB, only ~6 mg of sorbents was used. These results are very promising for extraction of Cs using magnetic core shell particles however further work is needed to understand the cycle stability, experiments using magnetic test loop and colloidal stability of Fe_3O_4@Co-PB.

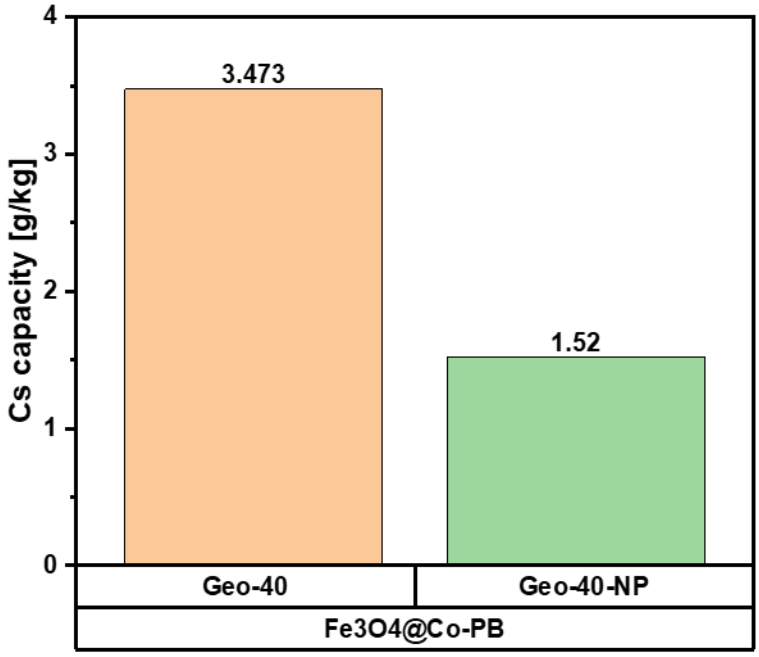

Figure 14. Cs adsorption capacities of Fe_3O_4@Co-PB in Geo-40 and Geo-40-NP

5.0 Literature Review of Antimony Removal

Sb is a naturally occurring element found in small amounts in the Earth's crust. It can enter water bodies through natural processes, as well as from industrial sources such as mining, smelting, and waste disposal. In most cases, dissociated Sb species exist in its oxyanion forms—antimonate ($Sb(OH)_6^-$) in oxic natural water bodies, and $Sb(OH)_3$ in anoxic water bodies. As has been verified by many studies, Sb can be harmful to humans and animals when ingested at high levels over a long period of time. Therefore, the U.S. Environmental Protection Agency (EPA) has set a maximum contaminant level (MCL) for Sb in drinking water of 6 ppb, based on the potential health effects of Sb, such as stomach pain, diarrhea, and vomiting (Regulations and Standards 1980). In addition to the EPA, other organizations, such as the World Health Organization and the European Union, also have regulations in place for Sb in drinking water. High levels of Sb in water can have acute effects on aquatic organisms like fish and invertebrates. Long-term exposure to lower levels of Sb would do harm to these organisms by disrupting their reproductive and growth processes. The toxicity of Sb can vary depending on its valence state. Antimony has several valence states, including -3, 0, +3, and +5, and Sb(III) is the most naturally abundant in environments. Sb(III) compounds are generally considered more toxic than Sb(V) compounds, because they can inhibit enzymes involved in important biological processes, can cause oxidative stress in cells, and can lead to further gastrointestinal symptoms, lung irritation, and skin irritation. Sb(V) is generally less toxic than trivalent antimony; but it can still have harmful effects on human health, including respiratory and cardiovascular effects, if exposure is prolonged or at high concentrations. Therefore, the removal of dissociated Sb from mining effluents before their release back to natural water is of great significance (Parker, Livshits, and McKeon 1979). Currently, the removal of Sb from aqueous systems can be achieved through various technologies (Ungureanu et al. 2015; Long et al. 2020).

5.1 Coagulation–Flocculation–Sedimentation

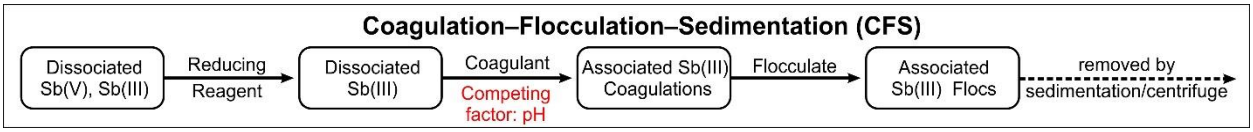

The coagulation–flocculation–sedimentation (CFS) process involves the addition of a coagulant, such as aluminum sulfate, ferric chloride (FC), and polyaluminum chloride to contaminated water to form larger particles that can be removed by sedimentation or filtration (Guo, Wu, and He 2009; Du et al. 2014; Y. Liu et al. 2019). This method provides a cost-effective way for removing Sb. For example, the CFS method using FC showed a dosing dependency of Sb(V) removal at room temperature under both a mild acidic condition (pH = 6.0 ± 0.2) and a weakly basic condition (pH = 7.8 ± 0.2) within a 0.2 ~ 1 mM FC dosing range. Nevertheless, the mild acidic condition showed a more complete removal at a given dosing condition and less dosing dependency than the weakly basic condition; whereas the removal of Sb(III) at room temperature within the same FC dosing range demonstrated a more complete removal under both basic and acidic conditions. Compared to Sb(V), the removal rate of Sb(III) showed less dependence on the dosing of FC, but the conclusion of the acidic condition outperforming the basic condition still stands.

5.2 Adsorption

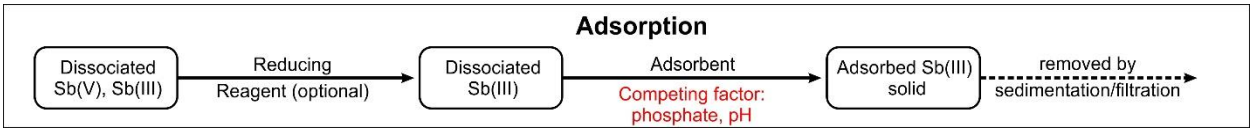

The adsorption method for the removal of Sb involves the use of various kinds of materials (such as alumina, goethite, biochar, etc.) to attract and bind Sb ions from the water. Kaolinite, as a classic material for the removal of heavy metals, manifested a good Sb sorption capability, especially under an acidic condition with a pH below 4, within which range the sorption rate of Sb(V) is close 100 percent, and gibbsite performed similarly comparing with kaolinite (Rakshit, Sarkar, and Datta 2015). But it is worth mentioning that the Sb(V) species undergoes competing absorption with phosphate species. The existence of phosphate species would significantly reduce the performance of kaolinite and gibbsite to less than half the sorption rate at the same acidic pH level, and Sb sorption could not be carried out at all when the pH is greater than 6. Such competing adsorption behavior is further studied with goethite as the sorbent (Xi et al. 2013). The study results suggested that the existence of Cl^-, SO_4^{2-}, and NO_3^- does not constitute competing adsorption, whereas PO_4^{3-} manifested a competing adsorption process. A synergistic effect toward Sb(V) adsorption was also observed using goethite in the presence of Fe(II) (Fan et al. 2016). This effect was attributed to the reduction of Sb(V) to Sb(III) by Fe(II), which improved the sorption capacity of Sb due to the lower solubility and migration of Sb(III) species. Furthermore, the sequence of addition also plays a role—adding Fe(II) prior to the addition of goethite to allow the Fe^{2+} cation to form a co-precipitation with Sb(V) would push the equilibrium concentration of remaining Sb(V) down to ~1/4 than using Fe(II) pre-absorbed goethite for the Sb sorption. The function of iron species was further studied by studying the adsorption of Sb onto iron oxyhydroxides (Guo et al. 2014). The affinities of Sb(V) and Sb(III) toward the iron oxide (as hydrous ferric oxide, HFO) were found to dependent on the Sb species, solution pH, and the characteristics of the iron oxides (Miao et al. 2014). Sb(V) adsorption onto the iron oxides benefited from the acidic condition, whereas Sb(III) adsorption was constant over a

broader pH range. Under acidic conditions, HFO showed the same affinity to both Sb(V) and Sb(III) species. However, HFO lost its affinity to Sb(V) under basic conditions while maintaining a good affinity to Sb(III). Other materials such as macro-/mesoporous alumina (Dou et al. 2015) and Manganese-functionalized biochar (Jia et al. 2020) were also found to have good Sb capacity, but their capacity dependence on pH varies due to their different binding energies.

5.3 Membrane Filtration

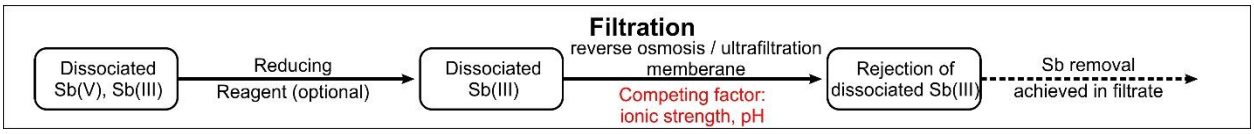

The filtration method for Sb removal involves the use of a membrane that separates dissociated Sb species from the water based on their size or charge differences, by reverse osmosis, nanofiltration, and ultrafiltration. For example, the polymer-assisted ultrafiltration process with a polyethersulfone membrane was employed for the removal of Sb, and it showed good rejection efficiency under acidic conditions (Ren et al. 2021). However, such efficiency is significantly affected by high ionic strength due to electric double-layer compressing and competition complexation. Similar to the results for the adsorption method, the existence of iron (as Fe hydrolytic flocs) increased the efficiency of ultrafiltration method for Sb removal, thanks to the same synergistic redox process between Fe and Sb species (Ma et al. 2017). On the other hand, the efficiency of the reverse osmosis (RO) method showed good dependence on the choice of membrane and the existing form of Sb (Kang et al. 2000). While the removal efficiency of Sb(V) is higher than that of Sb(III), the RO method showed pH independence relative to the removal of Sb(III), mainly due to the fast oxidation process of SB(III) to Sb(V).

5.4 Electrochemical Treatment

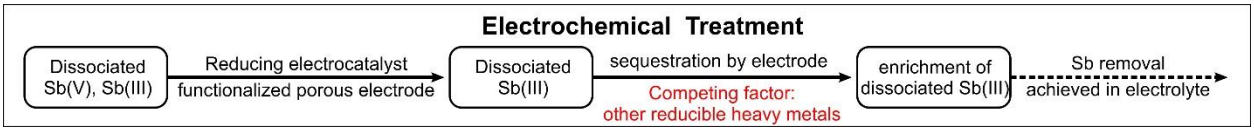

The use of an electrical overpotential to induce reactions that remove Sb ions from the water has been explored and was investigated together with light as the external stimuli. For example, it has been reported that MOF functionalized carbon nanotubes were used as the photoelectrochemical filtration system to carry out the oxidation-sequestration of Sb species (Li et al. 2020). A 97.7 ± 1.5 percent Sb(III) to Sb(V) transformation and a 92.9 ± 2.3 percent Sb total removal efficiency at 2.5 V and under illumination was reported for the hybrid material. Such a design is highly delicate and highly capable, but the selectivity of Sb species was not thoroughly investigated, and the industrial applicability of this approach has not been optimized.

5.5 Biological Treatment

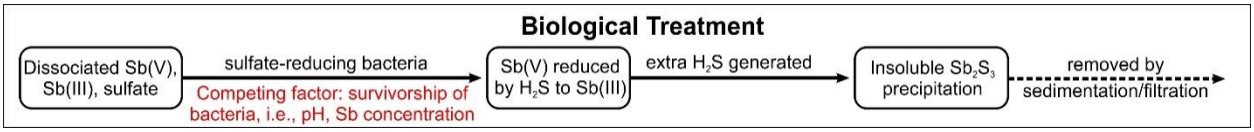

Certain microorganisms were reported to be capable of removing dissociated Sb species from water through bioremediation processes, which involve the metabolization and transformation of Sb compounds by bacteria or fungi (He et al. 2019). Sb species were removed through a cascade reduction-precipitation process in the presence of sulfate and sulfate-reducing bacteria (SRBs) (Wang et al. 2013; Zhang et al. 2016; Zhu et al. 2018). SRBs produces hydrogen sulfide by reducing sulfate, and the produced hydrogen sulfide is able to reduce Sb(V) to Sb(III). Then, the resulting Sb(III) reacts with the excess sulfide, resulting in the formation of insoluble antimony sulfide (Sb_2S_3) to be separated by precipitation. However, as effective as biological systems are, SRBs are delicate and could not survive in high Sb concentration environmental, under either strong acidic or basic conditions. When the presence of Sb exceeded 75 mg/L, SRBs' bioactivities were suppressed, leading to a huge decrease in Sb removal efficiency. Efforts were also made to use bio-produced hydrogen to reduce Sb species to achieve the removal of Sb (Lai et al. 2016).

It is also important to note that the effectiveness of each technology depends on factors such as the initial concentration of Sb in the water, the presence of other contaminants, and the cost and feasibility of the treatment method. Currently, CFS and the adsorption method are the most cost-effective approaches to removing dissociated Sb species from wastewater, but their lack of selectivity imposes more complicated pre-treatment of the wastewater and limits the effectiveness of their ability to remove Sb from natural water bodies. On the other hand, more delicate approaches such as biological treatment, electrochemical approaches, and membrane filtration presented good selectivity and efficiency, but their high energy consumption, high material manufacturing cost, and demanding operating environment have made them too expensive to be adopted for field applications. Therefore, cost-effective approaches of selectively extracting/removing dissociated Sb species from complicated environments remain to be explored.

6.0 Conclusion and Recommendations

In conclusion, PNNL developed a simple, continuous, and cost-effective magnetic core shell approach for extracting critical minerals from geothermal brine solutions. The same technology has been extended for Cs recovery from natural brine solutions received from our industrial partner. As part of this effort, PNNL identified, synthetized, and tested several sorbent materials that can act as a shell around the magnetic core to extract Cs from brine solution. Among all the materials tested, Co-PBs were found to exhibit the highest Cs adsorption capacity—reaching as high as 31.6 g/kg under neutral condition. The sorbent can be regenerated by simply washing it with HNO_3 or KCl to extract the Cs. Likewise, the Co-PB also exhibited extremely higher Cs adsorption capacities in Ohaaki brines with about a 98.3 percent of removal efficiency. A reasonable 6.1 percent IRR was estimated based on the measured Cs adsorption working capacity and some conservative economic assumptions. These results offered insights into the possibility of using PBs for selective removal of Cs from geothermal brines. Though our initial results are extremely promising, further work is needed to evaluate these materials in terms of improving Cs adsorption capacity, selectivity, sorbent evaluation in the magnetic test loop, the

cycle stability of the magnetic core coated with Co-PBs, and the polymer coated for magnetic core shell particle dispersion in solution. Further improve core-shell performance in terms of Cs adsorption capacity, selectivity under conditions relevant to geothermal brine is the key performance indicator for IRR analysis.

7.0 References

Elsaidi, Sameh K, Michael A Sinnwell, Arun Devaraj, Tim C Droubay, Zimin Nie, Vijayakumar Murugesan, B Peter McGrail, and Praveen K Thallapally. 2018. "Extraction of rare earth elements using magnetite@ MOF composites." *Journal of Materials Chemistry A* 6 (38): 18438-18443. https://doi.org/https://doi.org/10.1039/C8TA04750B.

Chiarizia, R, EP Horwitz, RA Beauvais, and SD Alexandratos. 1998. "Diphonix-CS: a novel combined cesium and strontium selective ion exchange resin." *Solvent extraction and ion exchange* 16 (3): 875-898. https://doi.org/https://doi.org/10.1080/07366299808934558.

Campbell, Emily L, Sandra K Fiskum, and Reid A Peterson. 2021. *Characterization of CST Post-Processing AP-105 Hanford Tank Waste.* Pacific Northwest National Lab.(PNNL), Richland, WA (United States).

Brown, Garrett N. 2014. "Literature review of spherical resorcinol-formaldehyde for cesium ion exchange."

Faustino, Patrick J, Yongsheng Yang, Joseph J Progar, Charles R Brownell, Nakissa Sadrieh, Joan C May, Eldon Leutzinger, David A Place, Eric P Duffy, and Florence Houn. 2008. "Quantitative determination of cesium binding to ferric hexacyanoferrate: Prussian blue." *Journal of pharmaceutical and biomedical analysis* 47 (1): 114-125. https://doi.org/https://doi.org/10.1016/j.jpba.2007.11.049.

Thallapally, Praveen K, Radha Kishan Motkuri, Carlos A Fernandez, B Peter McGrail, and Ghorishi S Behrooz. 2010. "Prussian blue analogues for CO2 and SO2 capture and separation applications." *Inorganic chemistry* 49 (11): 4909-4915. https://doi.org/https://doi.org/10.1021/ic902397w.

Yang, Hee-Man, Ju Ri Hwang, Dong Yeop Lee, Kyu Beom Kim, Chan Woo Park, Hee Reyoung Kim, and Kune-Woo Lee. 2018. "Eco-friendly one-pot synthesis of Prussian blue-embedded magnetic hydrogel beads for the removal of cesium from water." *Scientific Reports* 8 (1): 11476. https://doi.org/https://doi.org/10.1038/s41598-018-29767-y.

Loos-Neskovic, C, S Ayrault, V Badillo, B Jimenez, E Garnier, M Fedoroff, DJ Jones, and B Merinov. 2004. "Structure of copper-potassium hexacyanoferrate (II) and sorption mechanisms of cesium." *Journal of solid state chemistry* 177 (6): 1817-1828. https://doi.org/https://doi.org/10.1016/j.jssc.2004.01.018.

Melo, Antonio FAA, Vitor AN Carvalho, Kamila C Pagnoncelli, and Frank N Crespilho. 2013. "Single microparticle applied in magnetic-switchable electrochemistry." *Electrochemistry communications* 30: 79-82.

C. Carvalho, Caio Lenon, Anna Thaise B. Silva, Roberto AS Luz, Gustavo Montgomery B Castro, Cleanio da Luz Lima, Valmor Roberto Mastelaro, Robson Rosa da Silva, Osvaldo N Oliveira Jr, and Welter Cantanhêde. 2018. "Development of Co3 [Co (CN) 6] 2/Fe3O4 bifunctional nanocomposite for clinical sensor applications." *ACS Applied Nano Materials* 1 (8): 4283-4293.

Liu, J., P. F. Martin, and B. P. McGrail. 2022. "Rare-Earth Element Extraction from Geothermal Brine Using Magnetic Core-Shell Nanoparticles-Techno-Economic Analysis (vol 89, 101938, 2021)." *Geothermics* 105. https://doi.org/ARTN 102526
10.1016/j.geothermics.2022.102526. <Go to ISI>://WOS:000860119000002.

Liu, Jian, Paul F Martin, and B Peter McGrail. 2021. "Rare-earth element extraction from geothermal brine using magnetic core-shell nanoparticles-techno-economic analysis." *Geothermics* 89: 101938. https://doi.org/https://doi.org/10.1016/j.geothermics.2020.101938.

Regulations, US Environmental Protection Agency. Office of Water, and Standards. 1980. *Ambient Water Quality Criteria for Antimony*.

Parker, C Leon, Efim Livshits, and Kathleen McKeon. 1979. *Antimony removal technology for mining industry wastewaters*. Vol. 1. Environmental Protection Agency, Office of Research and Development,[Office ….

Ungureanu, Gabriela, Sílvia Santos, Rui Boaventura, and Cidália Botelho. 2015. "Arsenic and antimony in water and wastewater: Overview of removal techniques with special reference to latest advances in adsorption." *Journal of environmental management* 151: 326-342. https://doi.org/https://doi.org/10.1016/j.jenvman.2014.12.051.

Long, Xiaojing, Xin Wang, Xuejun Guo, and Mengchang He. 2020. "A review of removal technology for antimony in aqueous solution." *Journal of Environmental Sciences* 90: 189-204. https://doi.org/https://doi.org/10.1016/j.jes.2019.12.008.

Guo, Xuejun, Zhijun Wu, and Mengchang He. 2009. "Removal of antimony (V) and antimony (III) from drinking water by coagulation–flocculation–sedimentation (CFS)." *Water research* 43 (17): 4327-4335. https://doi.org/https://doi.org/10.1016/j.watres.2009.06.033.

Du, Xing, Fangshu Qu, Heng Liang, Kai Li, Huarong Yu, Langming Bai, and Guibai Li. 2014. "Removal of antimony (III) from polluted surface water using a hybrid coagulation–flocculation–ultrafiltration (CF–UF) process." *Chemical Engineering Journal* 254: 293-301. https://doi.org/https://doi.org/10.1016/j.cej.2014.05.126.

Liu, Yuanli, Zimo Lou, Kunlun Yang, Zheni Wang, Chuchen Zhou, Yizhou Li, Zhen Cao, and Xinhua Xu. 2019. "Coagulation removal of Sb (V) from textile wastewater matrix with enhanced strategy: Comparison study and mechanism analysis." *Chemosphere* 237: 124494. https://doi.org/https://doi.org/10.1016/j.chemosphere.2019.124494.

Rakshit, Sudipta, Dibyendu Sarkar, and Rupali Datta. 2015. "Surface complexation of antimony on kaolinite." *Chemosphere* 119: 349-354. https://doi.org/https://doi.org/10.1016/j.chemosphere.2014.06.070.

Xi, Jianhong, Mengchang He, Kunpeng Wang, and Guizhi Zhang. 2013. "Adsorption of antimony (III) on goethite in the presence of competitive anions." *Journal of Geochemical Exploration* 132: 201-208. https://doi.org/https://doi.org/10.1016/j.gexplo.2013.07.004.

Fan, Jian-Xin, Yu-Jun Wang, Ting-Ting Fan, Fei Dang, and Dong-Mei Zhou. 2016. "Effect of aqueous Fe (II) on Sb (V) sorption on soil and goethite." *Chemosphere* 147: 44-51. https://doi.org/https://doi.org/10.1016/j.chemosphere.2015.12.078.

Guo, Xuejun, Zhijun Wu, Mengchang He, Xiaoguang Meng, Xin Jin, Nan Qiu, and Jing Zhang. 2014. "Adsorption of antimony onto iron oxyhydroxides: adsorption behavior and surface structure." *Journal of hazardous materials* 276: 339-345. https://doi.org/https://doi.org/10.1016/j.jhazmat.2014.05.025.

Miao, Yangyang, Feichao Han, Bingcai Pan, Yingjie Niu, Guangze Nie, and Lu Lv. 2014. "Antimony (V) removal from water by hydrated ferric oxides supported by calcite sand and polymeric anion exchanger." *Journal of environmental sciences* 26 (2): 307-314. https://doi.org/https://doi.org/10.1016/S1001-0742(13)60418-0.

Dou, Xiaomin, Dinesh Mohan, Xueqin Zhao, and Charles U Pittman Jr. 2015. "Antimonate removal from water using hierarchical macro-/mesoporous amorphous alumina." *Chemical Engineering Journal* 264: 617-624. https://doi.org/https://doi.org/10.1016/j.cej.2014.11.123.

Jia, Xiaocen, Jianwei Zhou, Jing Liu, Peng Liu, Lu Yu, Bing Wen, and Yu Feng. 2020. "The antimony sorption and transport mechanisms in removal experiment by Mn-coated

biochar." *Science of the Total Environment* 724: 138158. https://doi.org/https://doi.org/10.1016/j.scitotenv.2020.138158.

Ren, Long-Fei, Yuanxin Lin, Hongchen Song, Haoyu Sun, and Jiahui Shao. 2021. "Efficient removal of antimony from aqueous solution by sustainable polymer assisted ultrafiltration process." *Separation and Purification Technology* 263: 118418. https://doi.org/https://doi.org/10.1016/j.seppur.2021.118418.

Ma, Baiwen, Xing Wang, Ruiping Liu, William A Jefferson, Huachun Lan, Huijuan Liu, and Jiuhui Qu. 2017. "Synergistic process using Fe hydrolytic flocs and ultrafiltration membrane for enhanced antimony (V) removal." *Journal of Membrane Science* 537: 93-100. https://doi.org/https://doi.org/10.1016/j.memsci.2017.05.022.

Kang, Meea, Mutsuo Kawasaki, Sinya Tamada, Tasuku Kamei, and Yasumoto Magara. 2000. "Effect of pH on the removal of arsenic and antimony using reverse osmosis membranes." *Desalination* 131 (1-3): 293-298. https://doi.org/https://doi.org/10.1016/S0011-9164(00)90027-4.

Li, Mohua, Yanbiao Liu, Chensi Shen, Fang Li, Chong-Chen Wang, Manhong Huang, Bo Yang, Zhiwei Wang, Jianmao Yang, and Wolfgang Sand. 2020. "One-step Sb (III) decontamination using a bifunctional photoelectrochemical filter." *Journal of hazardous materials* 389: 121840. https://doi.org/https://doi.org/10.1016/j.jhazmat.2019.121840.

He, Mengchang, Ningning Wang, Xiaojing Long, Chengjun Zhang, Congli Ma, Qianyun Zhong, Aihua Wang, Ying Wang, Aneesa Pervaiz, and Jun Shan. 2019. "Antimony speciation in the environment: Recent advances in understanding the biogeochemical processes and ecological effects." *Journal of environmental sciences* 75: 14-39. https://doi.org/https://doi.org/10.1016/j.jes.2018.05.023.

Wang, Huawei, Fulong Chen, Shuyong Mu, Daoyong Zhang, Xiangliang Pan, Duu-Jong Lee, and Jo-Shu Chang. 2013. "Removal of antimony (Sb (V)) from Sb mine drainage: biological sulfate reduction and sulfide oxidation–precipitation." *Bioresource technology* 146: 799-802. https://doi.org/https://doi.org/10.1016/j.biortech.2013.08.002.

Zhang, Guoping, Xiaoxue Ouyang, Haixia Li, Zhiping Fu, and Jingjing Chen. 2016. "Bioremoval of antimony from contaminated waters by a mixed batch culture of sulfate-reducing bacteria." *International Biodeterioration & Biodegradation* 115: 148-155. https://doi.org/https://doi.org/10.1016/j.ibiod.2016.08.007.

Zhu, Yanping, Min Wu, Naiyun Gao, Wenhai Chu, Na An, Qiongfang Wang, and Shuaifeng Wang. 2018. "Removal of antimonate from wastewater by dissimilatory bacterial reduction: Role of the coexisting sulfate." *Journal of hazardous materials* 341: 36-45. https://doi.org/https://doi.org/10.1016/j.jhazmat.2017.07.042.

Lai, Chun-Yu, Li-Lian Wen, Yin Zhang, Shan-Shan Luo, Qing-Ying Wang, Yi-Hao Luo, Ran Chen, Xiaoe Yang, Bruce E Rittmann, and He-Ping Zhao. 2016. "Autotrophic antimonate bio-reduction using hydrogen as the electron donor." *Water research* 88: 467-474. https://doi.org/https://doi.org/10.1016/j.watres.2015.10.042.

Pacific Northwest National Laboratory

902 Battelle Boulevard
P.O. Box 999
Richland, WA 99354

1-888-375-PNNL (7665)

www.pnnl.gov